

# Linear Stability of Reversing a Car-trailer Combination

Levente Mihályi<sup>1\*</sup>, Dénes Takács<sup>2</sup>

<sup>1</sup> Department of Applied Mechanics, Faculty of Mechanical Engineering, Budapest University of Technology and Economics, Műegyetem rkp. 3, H-1111 Budapest, Hungary

<sup>2</sup> MTA-BME Research Group on Dynamics of Machines and Vehicles, Műegyetem rkp. 3, H-1111 Budapest, Hungary

\* Corresponding author, e-mail: [mihalyi@mm.bme.hu](mailto:mihalyi@mm.bme.hu)

Received: 21 July 2021, Accepted: 27 March 2023, Published online: 05 April 2023

## Abstract

In this paper, we investigate the reverse motion of a car-trailer combination. The single track model of the vehicle is used with quasi-static tire model to design a simple linear feedback controller that can achieve stable reversing motion along a straight path. The linear stability of the closed-loop system is analyzed by constructing stability charts in the plane of the control gains. The effect of the reversing speed of the vehicle on the stability is also shown. In order to validate the theoretical results, laboratory experiments are carried out using a small-scale vehicle and a conveyor belt.

## Keywords

car-trailer combination, rectilinear reversing, linear control, laboratory testing

## 1 Introduction

The development of autonomous vehicles turned the field of vehicle dynamics to be even more relevant. As the level of automation develops, the applied control algorithms start to operate in such formerly avoided parameter domains where the nonlinear properties of the vehicle system are relevant, see [1]. These enhanced motion controls also realize different path-following tasks that could not be or could hardly be done by human drivers [2]. Reversing a truck having trailers is one of these tasks.

The stability problem of trailers often leads to road accidents. Since badly chosen payload positions or the high towing speed may generate violent vibrations (so-called snaking motion) of the trailer, the dynamics of the car-caravan and truck-trailer combinations are deeply analyzed in the literature [3]. The critical speed corresponding to the linear stability boundary of the straight-line forward motion can be increased using optimal system parameters, while the stability of the reverse motion requires feedback control [4].

In this paper, we analyze the reverse motion of a car-trailer combination [5, 6]. The equations of motion of the single track vehicle model are derived by means of Kane's method, and a simple linear feedback controller is designed to stabilize the straight-line reverse motion. For the sake of simplicity, the time delay of the control loop is neglected in our study. Stability charts are constructed to analyze the effect of the reversing speed on the stable domain of

the control gains. A small-scale experimental rig is introduced, where the theoretical results can be validated and a more sophisticated path following control algorithm can be tested in the future.

## 2 Mechanical model

The single track model [7] is applied to analyze the lateral dynamics of the car-trailer combination (see Fig. 1). We investigate an in-plane motion, where  $(X, Y)$  denote the ground-fixed coordinate system and  $(x, y)$  are local

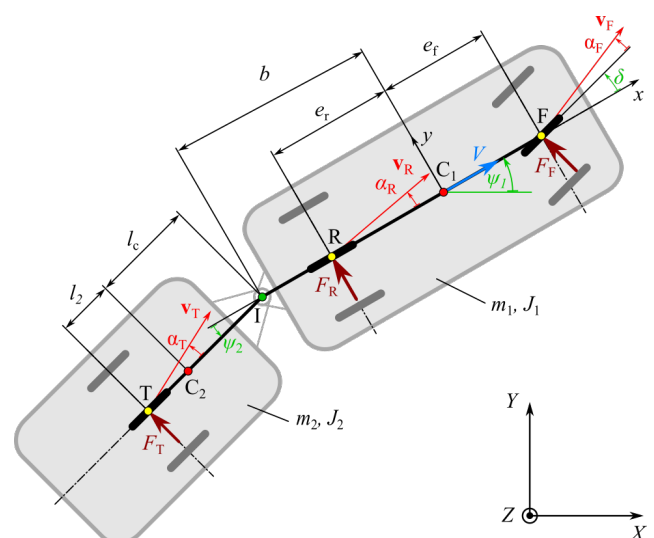


Fig. 1 Mechanical model with notations

coordinates fixed to the towing vehicle at its center of gravity  $C_1$ . Point  $C_2$  refers to the center of gravity of the trailer. The towing car and trailer are connected via a joint at point I. The geometric parameters are the following:  $e_f$  and  $e_r$  are the distances between  $C_1$  and the front and the rear axles respectively;  $b$  denotes the distance between  $C_1$  and the joint at I. The lengths  $l_c$  and  $l_2$  are defined between the center of gravity  $C_2$  and the joint I, and between the center of gravity  $C_2$  and the axle at T, respectively. The mass and the mass moment of inertia are represented by  $m_1, J_1$  for the car, and  $m_2, J_2$  for the trailer. The lateral forces  $F_F, F_R$ , and  $F_T$  are the tire forces, where subscripts refer to the points of actions. In our model, the self-aligning moments of the tires are neglected. The generalized coordinates of the system are the positions  $X$  and  $Y$  of the center of gravity  $C_1$ , the yaw angle  $\psi_1$  of the towing car, and the angle  $\psi_2$  of the trailer relative to the towing car, respectively. The steering angle of the towing vehicle is denoted by  $\delta$ , which is considered as a time-dependent input variable.

For the sake of simplicity, we set the longitudinal speed of the towing vehicle to be equal to the constant value  $V$ . This can be expressed as a kinematic constraint:

$$\dot{X} \cos \psi_1 + \dot{Y} \sin \psi_1 = V, \quad (1)$$

where dots refer to the derivatives with respect to time. Due to the presence of this kinematic constraint, the system is nonholonomic, and the equation of motion is determined using Kane's method [8]. The configuration of the system can be uniquely defined by four generalized coordinates, while the kinematic constraint reduces the number of variables that uniquely describe the velocity state by one. So, three suitably chosen pseudo velocities are needed:

$$\begin{aligned} \sigma_1 &:= -\dot{X} \sin \psi_1 + \dot{Y} \cos \psi_1, \\ \sigma_2 &:= \dot{\psi}_1, \\ \sigma_3 &:= \dot{\psi}_1 + \dot{\psi}_2, \end{aligned} \quad (2)$$

which are the lateral speed of the center of gravity  $C_1$ , the yaw rate of the towing vehicle and the yaw rate of the trailer. Expressing the generalized velocities from the linear system composed by Eq. (1) and Eq. (2), we obtain:

$$\begin{aligned} \dot{X} &= V \cos \psi_1 - \sigma_1 \sin \psi_1, \\ \dot{Y} &= V \sin \psi_1 + \sigma_1 \cos \psi_1, \\ \dot{\psi}_1 &= \sigma_2, \\ \dot{\psi}_2 &= \sigma_3 - \sigma_2. \end{aligned} \quad (3)$$

Besides them, three dynamic equations complete the equations of motion of the system based on Kane's method:

$$F_s + F_s^* = 0, \quad (4)$$

where the subscript  $s = 1, 2, 3$  refers to the  $s^{\text{th}}$  pseudo velocity.  $F_s$  and  $F_s^*$  are the nonholonomic generalized active forces and the nonholonomic generalized inertia forces.

In the case of a car-trailer combination these generalized forces are

$$\begin{aligned} F_s &= \left( \mathbf{F}_{\text{trailer}} \frac{\partial \mathbf{v}_{C_2}}{\partial \sigma_s} + \mathbf{M}_{C_{\text{trailer}}} \frac{\partial \boldsymbol{\omega}_2}{\partial \sigma_s} \right) + \left( \mathbf{F}_{\text{car}} \frac{\partial \mathbf{v}_{C_1}}{\partial \sigma_s} + \mathbf{M}_{C_{\text{car}}} \frac{\partial \boldsymbol{\omega}_1}{\partial \sigma_s} \right), \\ F_s^* &= - \left( m_1 \mathbf{a}_{C_1} \frac{\partial \mathbf{v}_{C_1}}{\partial \sigma_s} + \mathbf{J}_1 \boldsymbol{\varepsilon}_1 \frac{\partial \boldsymbol{\omega}_1}{\partial \sigma_s} \right) - \left( m_2 \mathbf{a}_{C_2} \frac{\partial \mathbf{v}_{C_2}}{\partial \sigma_s} + \mathbf{J}_2 \boldsymbol{\varepsilon}_2 \frac{\partial \boldsymbol{\omega}_2}{\partial \sigma_s} \right). \end{aligned} \quad (5)$$

In these formulas, the velocities read as

$$\begin{aligned} \mathbf{v}_{C_1} &= \begin{bmatrix} V \cos \psi_1 - \sigma_1 \sin \psi_1 \\ V \sin \psi_1 + \sigma_1 \cos \psi_1 \\ 0 \end{bmatrix}, \\ \mathbf{v}_1 &= \begin{bmatrix} V \cos \psi_1 - \sigma_1 \sin \psi_1 + \sigma_2 b \sin \psi_1 \\ V \sin \psi_1 + \sigma_1 \cos \psi_1 - \sigma_2 b \cos \psi_1 \\ 0 \end{bmatrix}, \\ \mathbf{v}_{C_2} &= \mathbf{v}_1 + \begin{bmatrix} \sigma_3 l_c \sin(\psi_1 + \psi_2) \\ -\sigma_3 l_c \cos(\psi_1 + \psi_2) \\ 0 \end{bmatrix}. \end{aligned} \quad (6)$$

The second and third pseudo velocities (cf. Eq. (2)) are defined as the angular velocities of the car and the trailer, thus, the partial derivatives can be easily expressed as:

$$\begin{aligned} \frac{\partial \boldsymbol{\omega}_1}{\partial \sigma_1} &= 0, \quad \frac{\partial \boldsymbol{\omega}_1}{\partial \sigma_3} = 0, \quad \frac{\partial \boldsymbol{\omega}_2}{\partial \sigma_1} = 0, \quad \frac{\partial \boldsymbol{\omega}_2}{\partial \sigma_2} = 0, \\ \frac{\partial \boldsymbol{\omega}_1}{\partial \sigma_2} &= \begin{bmatrix} 0 \\ 0 \\ 1 \end{bmatrix}, \quad \frac{\partial \boldsymbol{\omega}_2}{\partial \sigma_3} = \begin{bmatrix} 0 \\ 0 \\ 1 \end{bmatrix}. \end{aligned} \quad (7)$$

The forces and moments in Eq. (5) are

$$\begin{aligned} \mathbf{F}_{\text{trailer}} &= \mathbf{F}_T = \begin{bmatrix} -F_T \sin(\psi_1 + \psi_2) \\ F_T \cos(\psi_1 + \psi_2) \\ 0 \end{bmatrix}, \\ \mathbf{M}_{C_{\text{trailer}}} &= \mathbf{r}_{C_2, T} \times \mathbf{F}_T = \begin{bmatrix} 0 \\ 0 \\ -F_T l_2 \end{bmatrix}, \\ \mathbf{F}_{\text{car}} &= \mathbf{F}_F + \mathbf{F}_R = \begin{bmatrix} -F_F \sin(\psi_1 + \delta) - F_R \sin \psi_1 \\ F_F \cos(\psi_1 + \delta) + F_R \cos \psi_1 \\ 0 \end{bmatrix}, \\ \mathbf{M}_{C_{\text{car}}} &= \mathbf{r}_{C_1, F} \times \mathbf{F}_F + \mathbf{r}_{C_1, R} \times \mathbf{F}_R = \begin{bmatrix} 0 \\ 0 \\ F_F e_f \cos \delta - F_R e_r \end{bmatrix}. \end{aligned} \quad (8)$$

Substituting these back to the first expression of Eq. (5), the generalized active forces simplify to

$$\begin{aligned} F_1 &= F_F \cos \delta + F_R + F_T \cos \psi_2, \\ F_2 &= F_F e_f \cos \delta - F_T b \cos \psi_2 - F_R e_r, \\ F_3 &= -F_T (l_2 + l_c). \end{aligned} \quad (9)$$

According to the second expression of Eq. (5), the accelerations and angular accelerations of the car and the trailer are needed in order to calculate the generalized inertia forces. By definition, acceleration is the first derivative of velocity with respect to time, thus

$$\mathbf{a}_{C_1} = \frac{d\mathbf{v}_{C_1}}{dt}, \quad \boldsymbol{\varepsilon}_1 = \begin{bmatrix} 0 \\ 0 \\ \dot{\sigma}_2 \end{bmatrix}, \quad \mathbf{a}_{C_2} = \frac{d\mathbf{v}_{C_2}}{dt}, \quad \boldsymbol{\varepsilon}_2 = \begin{bmatrix} 0 \\ 0 \\ \dot{\sigma}_3 \end{bmatrix}. \quad (10)$$

For the sake of brevity, we do not spell out the formulas of the accelerations. But substituting the derivatives back to the second expression of Eq. (5), we obtain the generalized inertia forces:

$$\begin{aligned} F_1^* &= -(m_1 + m_2)(V\sigma_2 + \dot{\sigma}_1) - m_2 l_c \sigma_3^2 \sin \psi_2 + m_2 \dot{\sigma}_2 b \\ &\quad + m_2 \dot{\sigma}_3 l_c \cos \psi_2, \\ F_2^* &= m_2 b V \sigma_2 + m_2 b \dot{\sigma}_1 - m_2 b^2 \dot{\sigma}_2 - m_2 b \dot{\sigma}_3 l_c \cos \psi_2 \\ &\quad + m_2 b \dot{\sigma}_3 l_c \sin \psi_2 - J_1 \dot{\sigma}_2, \\ F_3^* &= -m_2 l_c \cos \psi_2 (-V\sigma_2 - \dot{\sigma}_1 + \dot{\sigma}_2 b) \\ &\quad - m_2 l_c \sin \psi_2 (-\sigma_1 \sigma_2 + \sigma_2^2 b) - m_2 l_c^2 \dot{\sigma}_3 - J_2 \dot{\sigma}_3. \end{aligned} \quad (11)$$

In summary, the nonlinear equations of motion – expressed by the generalized coordinates and the three pseudo velocities – are as follows:

$$\begin{aligned} (m_1 + m_2)(V\sigma_2 + \dot{\sigma}_1) + m_2 (l_c \sigma_3^2 \sin \psi_2 - \dot{\sigma}_2 b \\ - \dot{\sigma}_3 l_c \cos \psi_2) &= F_F \cos \delta + F_R + F_T \cos \psi_2, \\ m_2 b (-V\sigma_2 - \dot{\sigma}_1 + \dot{\sigma}_2 b + \dot{\sigma}_3 l_c \cos \psi_2 - \sigma_3^2 l_c \sin \psi_2) \\ + J_1 \dot{\sigma}_2 &= F_F e_f \cos \delta - F_R e_r - F_T b \cos \psi_2, \\ J_2 \dot{\sigma}_3 + m_2 l_c (-V\sigma_2 \cos \psi_2 - \dot{\sigma}_1 \cos \psi_2 - \sigma_1 \sigma_2 \sin \psi_2 \\ + \dot{\sigma}_2 b \cos \psi_2 + \sigma_2^2 b \sin \psi_2 + l_c \dot{\sigma}_3) &= -F_T (l_2 + l_c), \\ \dot{X} &= V \cos \psi_1 - \sigma_1 \sin \psi_1, \\ \dot{Y} &= V \sin \psi_1 + \sigma_1 \cos \psi_1, \\ \dot{\psi}_1 &= \sigma_2, \\ \dot{\psi}_2 &= \sigma_3 - \sigma_2, \end{aligned} \quad (12)$$

where the lateral forces  $F_F$ ,  $F_R$  and  $F_T$  are calculated based on the tire model.

We use a quasi-static tire model [7] considering small side slip angles ( $\alpha_F$ ,  $\alpha_R$ ,  $\alpha_T$ ), namely:

$$\begin{aligned} F_F &= -C_F \cdot \alpha_F, \\ F_R &= -C_R \cdot \alpha_R, \\ F_T &= -C_T \cdot \alpha_T, \end{aligned} \quad (13)$$

where the constants  $C_F$ ,  $C_R$  and  $C_T$  represent the so-called cornering stiffness of the tires. The side slip angles can be calculated via the lateral and longitudinal velocities of the wheel's center points, which read:

$$\begin{aligned} \alpha_F &= \left( \tan^{-1} \left( \frac{\sigma_1 + e_f \sigma_2}{V} \right) - \delta \right) \text{sgn} V, \\ \alpha_R &= \tan^{-1} \left( \frac{\sigma_1 - e_r \sigma_2}{V} \right) \text{sgn} V, \\ \alpha_T &= \text{sgn} (V + (l_2 + l_c) \sigma_3 \sin \psi_2) \\ &\quad \times \left[ \tan^{-1} \left( \frac{\sigma_1 - b \sigma_2 - (l_2 + l_c) \sigma_3 \cos \psi_2}{V + (l_2 + l_c) \sigma_3 \sin \psi_2} \right) - \psi_2 \right]. \end{aligned} \quad (14)$$

Here, the sign function is applied for the longitudinal speeds of the wheel center points to handle both the forward and the reverse motions of the vehicle (positive/negative value of longitudinal speed  $V$ ) with the same mathematical formulas. For example, see Fig. 2 for the interpretation of the side slip angle of the car's rear wheel in forward (Fig. 2 (a)) and in reverse (Fig. 2 (b)) motions.

Note, the so-called kinematic model, which considers rigid wheels with point contact, could be an alternative model for the analysis. However, in the case of a fully loaded truck–trailer combination, the dynamic model is more appropriate due to the relatively large tire deformations evolving when the vehicle turns. Accounting the tire deformations may have even more importance when the truck and/or the trailer have multiple axles.

### 3 Control

Since the reverse motion along a straight path is linearly unstable without control, a controller is designed in this section. The yaw angle of the car ( $\psi_1$ ) and the relative

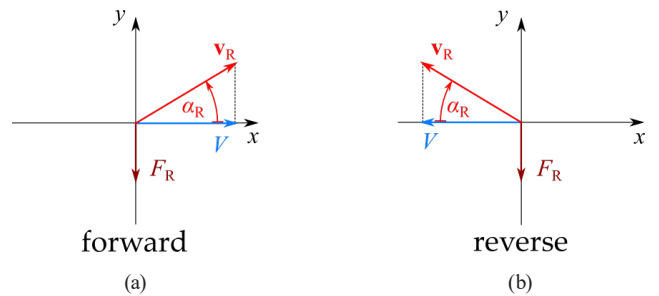


Fig. 2 Side slip angles in forward (a) and reverse (b) motions

angle of the trailer ( $\psi_2$ ), and the lateral position of the car ( $Y$ ) are utilized as feedback:

$$\delta = -P_{\psi_1}\psi_1 - P_{\psi_2}\psi_2 - P_Y Y, \quad (15)$$

where  $P_{\psi_1}$ ,  $P_{\psi_2}$  and  $P_Y$  denote the control gains.

First, we linearize the equations of motion about the straight motion of the car-trailer combination. As we want to analyze the closed-loop system, the equations of motion are arranged into the general state-space representation form:

$$\dot{\mathbf{x}} = \mathbf{A} \cdot \mathbf{x} + \mathbf{B} \cdot \mathbf{u}, \quad (16)$$

where

$$\mathbf{u} = \mathbf{K} \cdot \mathbf{x} \quad (17)$$

is the input vector,  $\mathbf{A}$  denotes the system matrix,  $\mathbf{B}$  is the input matrix, and  $\mathbf{x}$  means the state vector:

$$\mathbf{x} = [\sigma_1 \quad \sigma_2 \quad \sigma_3 \quad Y \quad \psi_1 \quad \psi_2]^T. \quad (18)$$

The system matrix can be expressed as  $\mathbf{A} = \mathbf{M}^{-1}\mathbf{D}$ . Detailed  $\mathbf{M}$ ,  $\mathbf{D}$ ,  $\mathbf{B}$  and  $\mathbf{K}$  matrices are given in the Appendix.

Using the state-space representation, we can examine the linear stability of the system by means of the characteristic roots of the characteristic equation

$$\det(\mathbf{I} \cdot \lambda - (\mathbf{M}^{-1} \cdot (\mathbf{D} + \mathbf{B} \cdot \mathbf{K}))) = 0, \quad (19)$$

where  $\mathbf{I}$  denotes the identity matrix. The straight motion of the vehicle is unstable if and only if the real part of the rightmost characteristic root becomes positive. We distinguish two types of instability [9]: static loss of stability happens if the imaginary part of the critical root is zero ( $\lambda = 0$ ), which is at  $P_Y = 0$ . Dynamic loss of stability takes place for nonzero imaginary part ( $\lambda = \pm i\omega$ ). In this latter case, Hopf bifurcation may happen and stable or unstable periodic solutions occur around the straight motion depending on the sense (supercritical/subcritical) of the Hopf bifurcation. To detect the stability boundary, we use the bisection method [10], by which we determine the critical parameter setups, for which, characteristic roots are situated on the imaginary axis of the complex plane. These calculations can be done analytically, but the relatively high-dimensional matrices would lead to excessive algebraic complexity. Therefore, stability charts are constructed by numerical calculations in our paper. The parameter values in Table 1 belong to a common car-trailer combination.

The stability charts are shown in Fig. 3, where stability boundaries are plotted in the separated panels for four different values of the  $P_{\psi_2}$  gain. For each of these setups, three different values of longitudinal speed are considered.

**Table 1** Numerical values of the system parameters

Parameter	Value	Unit
$m_1$	1300	kg
$m_2$	400	kg
$J_1$	1500	kg m <sup>2</sup>
$J_2$	160	kg m <sup>2</sup>
$e_f$	1.4	m
$e_r$	1.6	m
$b$	1.8	m
$l_c$	0.7	m
$l_2$	1.3	m
$C_F, C_R, C_T$	20000	N/rad

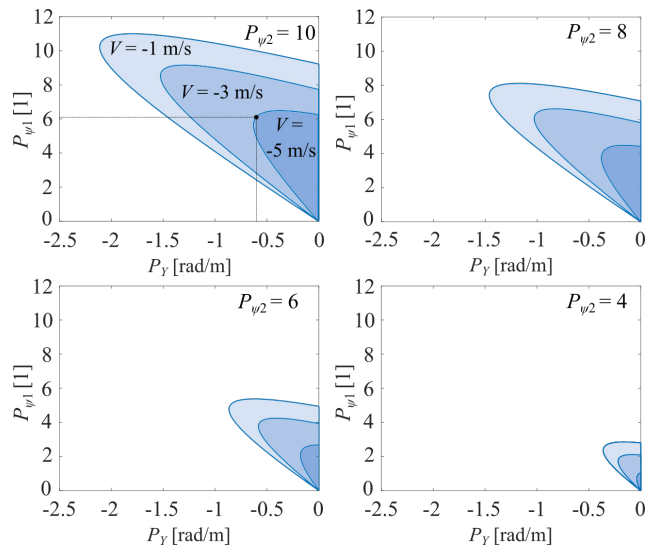


**Fig. 3** Stability charts with different fixed gains of the second proportional term

The blue areas denote the parameter domains of the control gains for which the straight reverse motion of the vehicle system is stable. As it can be observed, both the reversing speed  $V$  and the control gain  $P_{\psi_2}$  of the trailer's relative angle have significant effects on the area of the stable domain: faster reversing speed, and lower gain values lead to smaller stable domains.

Tuning feedback gains can be achieved by different procedures. Linear Quadratic Regulator (LQR) is a commonly used method, which would have been applied in our case as well. However, constructing stability charts is a suitable method for investigating the effect of different parameters on stability, e.g., the geometrical parameters, the longitudinal speed, or the time delay occurring in the feedback control loop.

A possible measure of the performance of the control is the real part of the rightmost characteristic root. Namely, the more negative this real part is, the more stable the

system is. For the  $P_{\psi_2} = 10$ ,  $V = 1$  m/s case (left top panel in Fig. 3), the most stable parameter point is marked with black dot at  $P_Y = -0.6566$  rad/m and  $P_{\psi_1} = 6.182$ .

#### 4 Experimental test

In order to validate our theoretical results on the stability of the controlled reverse motion of the vehicle, laboratory experiments were carried out. The small-scale test rig of [11] was used, in which a 1:10 vehicle model can be controlled on a treadmill. The car-trailer system was constructed as shown in Fig. 4. The car is attached to the frame of the treadmill by a 5 degrees-of-freedom suspension that only constrains the longitudinal speed of the car. The positions and orientations of the car and trailer are measured via linear encoders and magnetic rotary sensors. These signals are acquired by a NI cRIO unit, and the steering of the car is controlled based on the control law in Eq. (15).

The parameter values of the small-scale vehicle model are shown in Table 2. We present the experimental results for the speed of 0.3 m/s and for  $P_{\psi_2} = 10$ . The comparison between the theoretical stability boundary and the experimental test results is shown in Fig. 5.

The blue area is the theoretically stable domain. According to the test results, unstable points are marked with red crosses, and stable points refer to green dots.

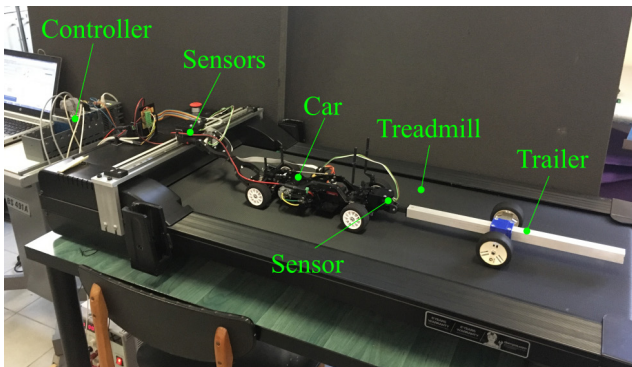


Fig. 4 Experimental setup

Table 2 Numerical values of the system parameters of the test

Parameter	Value	Unit
$m_1$	0.92	kg
$m_2$	0.4	kg
$J_1$	0.009	kg m <sup>2</sup>
$J_2$	0.0013	kg m <sup>2</sup>
$e_f$	0.1	m
$e_r$	0.14	m
$b$	0.19	m
$l_c$	0.2	m
$l_2$	0.02	m
$C_F, C_R, C_T$	50	N/rad

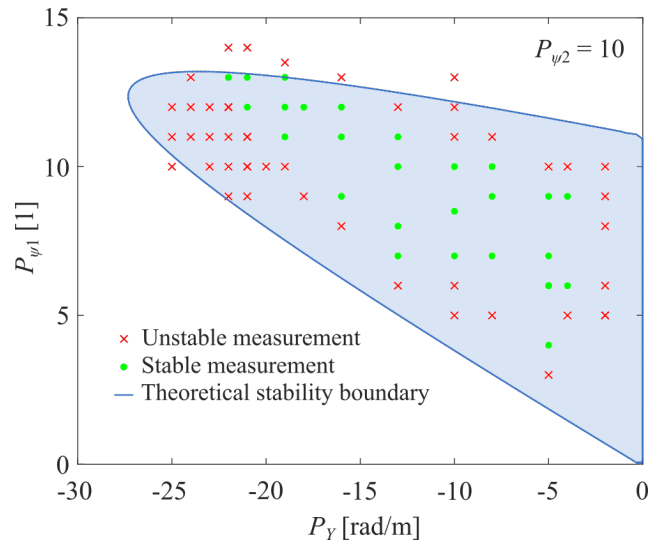


Fig. 5 Measurement points compared to the theoretical (blue curve) stability boundary

Although measurements provide a somewhat smaller stable domain, a good qualitative agreement can be established. The shape of the practical stability boundary suggested by the measurement points follows the theoretical one. However, some reasons can be mentioned related to the quantitative mismatch. Dry friction is not modeled in this research, so this phenomenon would modify the stable area, especially in the low-gain domain. On the other hand, time delay affects stability as well. Although the static stability boundary remains at  $P_Y = 0$  – since time delay has no effect on the  $\lambda = 0$  case –, another dynamic stability boundary may appear due to the delay, shrinking the area. The exponential filtering of the measured signals may introduce relevant time delay in the control loop of our experiment, but accounting for this time delay is planned to be a future task of our research.

Stability charts in Fig. 3 show that it would be considerable to raise the fixed control gain to reach better performance. However, small-scale tests proved that using extremely high gains causes unstable motions. This fact also suggests that the time delay may have a relevant effect.

The straight reverse motion of the vehicle can be stabilized by the designed controller using control gains chosen from the middle of the theoretically predicted stable domain.

#### 5 Conclusion

A simple linear feedback controller was presented for reversing a car-trailer combination. The controller was designed based on the single-track vehicle model of the car-trailer combination considering quasi-static tire model. It was shown that the straight reverse motion of the vehicle can be stabilized by feeding back the lateral position of the car, the yaw

angle of the car and the relative angle of the trailer. We examined the effects of the vehicle speed on the stability, and validated our results via small-scale laboratory experiments.

The constructed mechanical model of the paper and the designed small-scale experimental rig serve as a good basis for our future analyses on the effect of the feedback delay of the controller [12]. It is also intended to realize the path-following of the vehicle system [13, 14] in order to extend the straight-line motion to more complicated ones, e.g., making a lane change smoothly.

### References

[1] Rossa, F. D., Mastinu, G., Piccardi, C. "Bifurcation analysis of an automobile model negotiating a curve", *Vehicle System Dynamics*, 50(10), pp. 1539–1562, 2012.  
<https://doi.org/10.1080/00423114.2012.679621>

[2] Goh, J. Y., Goel, T., Christian Gerdes, J. "Toward Automated Vehicle Control Beyond the Stability Limits: Drifting Along a General Path", *Journal of Dynamic Systems, Measurement and Control*, 142(2), 021004, 2020.  
<https://doi.org/10.1115/1.4045320>

[3] Darling, J., Tilley, D., Gao, B. "An experimental investigation of car—trailer high-speed stability", *Proceedings of the Institution of Mechanical Engineers, Part D: Journal of Automobile Engineering*, 223(4), pp. 471–484, 2009.  
<https://doi.org/10.1243/09544070JAUTO981>

[4] Tilbury, D., Murray, R. M., Shankar Sastry, S. "Trajectory generation for the N-trailer problem using Goursat normal form", *IEEE Transactions on Automatic Control*, 40(5), pp. 802–819, 1995.  
<https://doi.org/10.1109/9.384215>

[5] Roh, J., Chung, W. "Reversing Control of a Car with a Trailer Using the Driver Assistance System", *International Journal of Advanced Robotic Systems*, 8(2), 2011.  
<https://doi.org/10.5772/10578>

[6] Altafini, C., Speranzon, A., Wahlberg, B. "A feedback control scheme for reversing a truck and trailer vehicle", *IEEE Transactions on Robotics and Automation*, 17(6), pp. 915–922, 2001.  
<https://doi.org/10.1109/70.976025>

[7] Pacejka, H. B. "Tyre and Vehicle Dynamics", 3<sup>rd</sup> ed., Butterworth–Heinemann, 2012. ISBN 978-0-08-097016-5  
<https://doi.org/10.1016/C2010-0-68548-8>

### Acknowledgement

The research reported in this paper and carried out at BME has been supported by the National Research, Development and Innovation Office under grant no. NKFI-128422 and by the NRDI Fund (TKP2020 IES, Grant No. BME-IE-MIFM and TKP2020 NC, Grant No. BME-NC) based on the charter of bolster issued by the NRDI Office under the auspices of the Ministry for Innovation and Technology.

[8] Kane, T. R., Levinson, D. A. "Dynamics: Theory and Applications", McGraw-Hill Book Company, 1985. ISBN 0070378460 [online] Available at: <https://ecommons.cornell.edu/handle/1813/638> [Accessed: 17 March 2023]

[9] Hac, A., Fulk, D., Chen, H. "Stability and Control Considerations of Vehicle-Trailer Combination", *SAE International Journal of Passenger Cars – Mechanical Systems*, 1(1), pp. 925–937, 2009.  
<https://doi.org/10.4271/2008-01-1228>

[10] Bachrathy, D., Stépán, G. "Bisection method in higher dimensions and the efficiency number", *Periodica Polytechnica Mechanical Engineering*, 56(2), pp. 81–86, 2012.  
<https://doi.org/10.3311/pp.me.2012-2.01>

[11] Vörös, I., Turányi, L., Várszegi, B., Takács, D. "Small-scale Experimental Test Rig for Lateral Vehicle Control", *Periodica Polytechnica Mechanical Engineering*, 65(2), pp. 163–170, 2021.  
<https://doi.org/10.3311/PPme.17269>

[12] Insperger, T., Stépán, G. "Semi-Discretization for Time-Delay Systems: Stability and Engineering Applications", Springer, 2011. ISBN 978-1-4614-0334-0  
<https://doi.org/10.1007/978-1-4614-0335-7>

[13] Nakamura, Y., Ezaki, H., Tan, Y., Chung, W. "Design of Steering Mechanism and Control of Nonholonomic Trailer Systems", *IEEE Transactions on Robotics and Automation*, 17(3), pp. 367–374, 2001.  
<https://doi.org/10.1109/70.938393>

[14] Bertolazzi, E., Frego, M. "On the  $G^2$  Hermite Interpolation Problem with Clothoids", *Journal of Computational and Applied Mathematics*, 341, pp. 99–116, 2018.  
<https://doi.org/10.1016/j.cam.2018.03.029>

### Appendix

The matrices mentioned in Section 3 are

$$M = \begin{bmatrix} m_1 + m_2 & -m_2 b & -m_2 l_c & 0 & 0 & 0 \\ -m_2 b & J_1 + m_2 b^2 & m_2 b l_c & 0 & 0 & 0 \\ -m_2 l_c & m_2 b l_c & J_2 + m_2 l_c^2 & 0 & 0 & 0 \\ 0 & 0 & 0 & 1 & 0 & 0 \\ 0 & 0 & 0 & 0 & 1 & 0 \\ 0 & 0 & 0 & 0 & 0 & 1 \end{bmatrix};$$

$$D = \begin{bmatrix} d_{11} & d_{12} & d_{13} & 0 & 0 & C_T \operatorname{sgn}(V) \\ d_{21} & d_{22} & d_{23} & 0 & 0 & -C_T b \operatorname{sgn}(V) \\ d_{31} & d_{32} & d_{33} & 0 & 0 & -C_T (l_2 + l_c) \operatorname{sgn}(V) \\ 1 & 0 & 0 & 0 & V & 0 \\ 0 & 1 & 0 & 0 & 0 & 0 \\ 0 & -1 & 1 & 0 & 0 & 0 \end{bmatrix},$$

where

$$d_{11} = \frac{-C_F - C_R - C_T}{V} \operatorname{sgn}(V),$$

$$d_{12} = \frac{(-C_F e_f + C_R e_r + C_T b) \operatorname{sgn}(V) - (m_1 + m_2) V^2}{V},$$

$$d_{13} = \frac{C_T (l_2 + l_c)}{V} \operatorname{sgn}(V),$$

$$d_{21} = \frac{-C_F e_f + C_R e_r + C_T b}{V} \operatorname{sgn}(V),$$

$$d_{22} = \frac{(-C_F e_f^2 - C_R e_r^2 - C_T b^2) \operatorname{sgn}(V) + V^2 m_2 b}{V},$$

$$d_{23} = \frac{-C_T (l_2 + l_c) b}{V} \operatorname{sgn}(V),$$

$$d_{31} = \frac{C_T (l_2 + l_c)}{V} \operatorname{sgn}(V),$$

$$d_{32} = \frac{-C_T (l_2 + l_c) b \operatorname{sgn}(V) + V^2 m_2 l_c}{V},$$

$$d_{33} = \frac{-C_{aT} (l_2 + l_c)^2}{V} \operatorname{sgn}(V);$$

$$\mathbf{B} = \begin{bmatrix} 0 & 0 & 0 & C_F & C_F & C_F \\ 0 & 0 & 0 & C_F e_f & C_F e_f & C_F e_f \\ 0 & 0 & 0 & 0 & 0 & 0 \\ 0 & 0 & 0 & 0 & 0 & 0 \\ 0 & 0 & 0 & 0 & 0 & 0 \\ 0 & 0 & 0 & 0 & 0 & 0 \end{bmatrix} \operatorname{sgn} V;$$

$$\mathbf{K} = \begin{bmatrix} 0 & 0 & 0 & 0 & 0 & 0 \\ 0 & 0 & 0 & 0 & 0 & 0 \\ 0 & 0 & 0 & 0 & 0 & 0 \\ 0 & 0 & 0 & -P_Y & 0 & 0 \\ 0 & 0 & 0 & 0 & -P_{\psi_1} & 0 \\ 0 & 0 & 0 & 0 & 0 & -P_{\psi_2} \end{bmatrix}.$$